A unified scaling model for flow through a lattice of microfabricated posts†

Nimisha Srivastava,* Changsong Din, Andrew Judson, Noel C. MacDonald and Carl D. Meinhart

Received 25th September 2009, Accepted 14th December 2009
First published as an Advance Article on the web 9th February 2010
DOI: 10.1039/b919942j

A scaling model is presented for low Reynolds number viscous flow within an array of microfabricated posts. Such posts are widely used in several lab-on-a-chip applications such as heat pipes, antibody arrays and biomolecule separation columns. Finite element simulations are used to develop a predictive model for pressure driven viscous flow through posts. The results indicate that the flow rate per unit width scales as $\sim h^{1.17} g^{1.33}/d^{0.5}$ where h is the post height, d post diameter and g is the spacing between the posts. These results compare favorably to theoretical limits. The scaling is extended to capillary pressure driven viscous flows. This unified model is the first report of a scaling that incorporates both viscous and capillary forces in the microfabricated post geometry. The model is consistent with Washburn dynamics and was experimentally validated to within 8% using wetting on microfabricated silicon posts.

Introduction

Microfabrication techniques are commonly used to make a variety of unique geometries for microfluidic applications. One such geometry is a lattice of microfabricated posts. Microfabricated posts have been used to make a particle array trap using negative dielectrophoresis force and hydrodynamic force,[1] where the cells are trapped at the stagnation points of the cylindrical posts. An assembly of microposts has also been used for the separation and isolation of rare tumor-derived epithelial cells from whole blood samples of cancer patients.[2] An array of posts has also been used in capillary electrochromatography separation[3] and in micro-heat pipes.

Despite the wide use of microfabricated posts, no universal scaling law exists for predicting flow around these posts. Previous investigations have been limited to idealized geometries. For example, flow past an isolated, infinitely long cylinder can be approximated using matched asymptotic analysis.[4] Flow past a single isolated cylinder has also been extended to a square array of infinitely long cylinders.[5] While the solutions to these idealized problems provide some guidelines for understanding the flow within a lattice of posts, they cannot be used to engineer lab-on-a-chip devices. The problem of flow within an assembly of posts used in microfluidic applications differs from the problem of flow around an infinitely long cylinder in that microposts are bounded on at least one side by the supporting substrate. Ishino *et al.* have made accurate predictions in the two extreme regimes when either the drag from the post surface (tall posts) or the drag from the bottom surface dominates (short posts) and have also validated these predictions by experiments.[6] They have shown that for short posts ($h < p$, center-to-center distance), the speed of wetting increases as the height of the post increases, while for tall posts ($h > p$), the speed of wetting is fixed by the radius of the posts.

Department of Mechanical Engineering, University of California Santa Barbara, CA 93106, USA

† Electronic supplementary information (ESI) available: Details of derivations. See DOI: 10.1039/b919942j

In the present work, a combination of finite element modeling, dimensional analysis, and wetting experiments are used to develop and validate a predictive scaling law for flow through an array of finite microfabricated posts that are in contact with a supporting substrate. The viscous scaling model accounts for viscous resistance from both the pillar surface and supporting substrate, and is valid over a wide spectrum of post geometries. The viscous scaling model is combined with surface energy-based estimates of the capillary pressure to obtain a unified scaling law that is analogous to Washburn dynamics. Finally, wetting experiments were performed on microfabricated silicon posts, which agree to within 10% of the scaling law for a single contact angle.

Theory and modeling

The flow through a lattice of microfabricated posts is analogous to Washburn dynamics, which describes the interaction between surface tension and viscous forces during the wetting of a circular capillary.[7] According to Washburn dynamics, the distance, l penetrated by a liquid driven by capillary pressure into a horizontal tube is given as $l = \sqrt{\frac{\gamma r t \cos\theta}{2\mu}}$ or $l = \sqrt{Dt}$ where $D = \sqrt{\frac{\gamma r \cos\theta}{2\mu}}$, γ is the liquid surface tension, t is the time, r is radius of the capillary, θ the contact angle and μ the liquid viscosity. The coefficient of penetrance, D, measures the ability of the liquid to penetrate a capillary tube or, in our case, a lattice of posts.

The microfabricated post geometry is shown in Fig. 1. The height of the posts is given by h, diameter d, and gap between the posts g. We seek to find an analogous expression for penetrance D in terms of the geometric parameters h, d, and g.

An expression for the capillary pressure in the microfabricated post structure shown in Fig. 1 can be obtained by comparing the difference in surface energy between wetted posts (dE_{wetted}) and dry posts ($dE_{\text{non-wetted}}$). This difference between surface energies ($dE_{\text{non-wetted}} - dE_{\text{wetted}}$) drives liquid wetting, to obtain a minimal

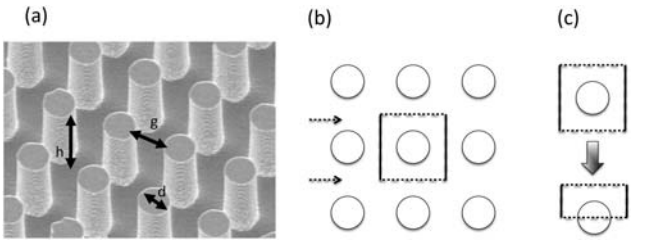

Fig. 1 Image of the device and sketch for the numerical model. **(a)** The Figure shows an array of posts microfabricated in silicon. The posts are 5 μm in diameter, 45 μm high and 5 μm apart. **(b)** An array of posts may be simulated by considering flow around an isolated pillar. In this case, flow was simulated around the center pillar. The black box around the center post indicates the control volume or the computation domain. Symmetry boundary condition is applied on the boundary shown with dotted lines. Periodic boundary conditions of flow rate are applied on the other two boundaries shown in solid lines. Dotted arrow shows the direction of flow. **(c)** Due to the inherent symmetry in the problem, the computation domain can be further halved. Image of the corresponding 3-d model in COMSOL is shown in Fig. 3.

energy state. By considering the change in surface energy of the wetting liquid front by a small wetting distance dx through the pillars, an expression for capillary pressure can be derived

$$\Delta P_{cap} = \frac{\gamma}{p^2 h}\left[\cos\theta\left(\pi d h + p^2 - \frac{\pi d^2}{4}\right) - \left(p^2 - \frac{\pi d^2}{4}\right)\right] \quad (1)$$

where the pitch is $p = g + d$ (*i.e.* center-to-center distance between the posts). See Supplemental **A**† or elsewhere for details.[6]

A universal expression for viscous losses through the microfabricated post structure cannot be derived easily from first principles. This expression must account for viscous drag from the posts, interactions between the posts, and viscous losses from the supporting substrate. As a result, a combination of finite-element simulations and dimensional analysis is used to derive a scaling law that is applicable to a large range of the geometric parameters.

We define a dimensionless flow rate per unit width, $\hat{q}$, using the flow rate per unit gap, q, viscosity, μ, and the driving pressure gradient dP/dx (see Supplemental **C** for details†). The pillar geometry has *three* independent parameters, d, g and h—therefore, $\hat{q}$ can be expressed arbitrarily as a function of two dimensionless parameters, h/g and g/d.

$$\hat{q} = \frac{3\mu q}{\left(dP/dx\right)pd^2} = \psi\left(\frac{h}{g}, \frac{g}{d}\right) \quad (2)$$

The function $\psi\left(\frac{h}{g}, \frac{g}{d}\right)$ can be determined by numerically simulating the simplified geometry shown in Fig. 1c. The numerical simulations are conducted using COMSOL V3.5a (COMSOL, Inc., Stockholm, Sweden). For ease of computation and faster convergence, a single isolated post with appropriate boundary conditions (symmetry, periodic and no-slip) is used to simulate the lattice of posts as shown in Fig. 2. The numerical model uses the weak formulation of the incompressible Navier–Stokes equation

$$\rho(u.\nabla)u = \nabla\bullet[-pI + \mu(\nabla u + (\nabla u)^T)] \text{ and } \nabla.u = 0$$

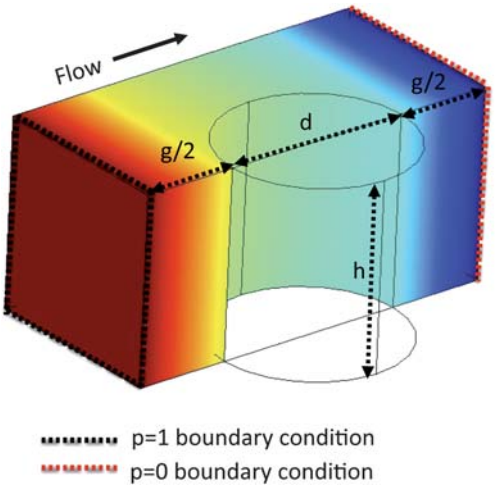

Fig. 2 Image of the numerical model. The Figure shows the computation domain used in the numerical model to simulate pressure driven flow around an array of posts (3-d rendering of the sketch shown in Fig. 1c). No-slip boundary condition is applied on the bottom surface. Pressure boundary conditions are applied upstream and downstream at a distance $g/2$ from the post as shown in the Figure. Symmetry boundary condition is applied on all remaining surfaces.

In order to obtain flow profiles for a wide range of post geometry (h, d, p), at least an order of magnitude in each of these, the N–S equations are made dimensionless using the diameter of the post. A parametric solver is used to scan the heights h, while holding d and p constant. The Moving Mesh (ALE) application mode is used for scanning the parameters d and p by mapping each geometry into a baseline finite element geometry. See Supplemental **D** for details.†

To obtain $\hat{q}$, the numerical model is used to compute the flow rate per unit gap, q, around the post for a given pressure drop. $\hat{q}$ is then calculated using eqn (2) for combinations of g, d and h. The diameter, d, is varied between 5 μm and 100 μm. The non-dimensional parameters g/d and h/g are varied between 1 and 10. Fig. 3a shows the plot of $\hat{q}$as a function of h/g for $g/d = 1$, 4 & 10. The data collapses onto a single curve to obtain the universal scaling shown in Fig. 3b, where

$$\hat{q} = \frac{3\mu q}{\left(dP/dx\right)pd^2} = \psi\left(\frac{h}{g}, \frac{g}{d}\right) = 10\left(\frac{h}{g}\right)^{1.17}\left(\frac{g}{d}\right)^{2.5}$$

Rearranging, the following expression is obtained for the flow rate per unit width.

$$q = \frac{\left(dP/dx\right)}{30\mu}\,\frac{ph^{1.17}g^{1.33}}{d^{0.5}} \quad (3)$$

Eqn (3) is accurate to within 8% over the parameter space $g/d \sim 10$ and $1 < h/g < 10$. As the posts get closer (*i.e.*, for $g/d \sim 1$ and $1 < h/g < 10$), the error increases slightly but is still within 10%.

Limiting scenarios of eqn (3) were examined to better understand the relevance of the exponents of h, d and g. When $g \ll h$ and $g \ll d$, the limit of lubrication flow is obtained for which the flow rate is given by[8] (see Fig. 4)

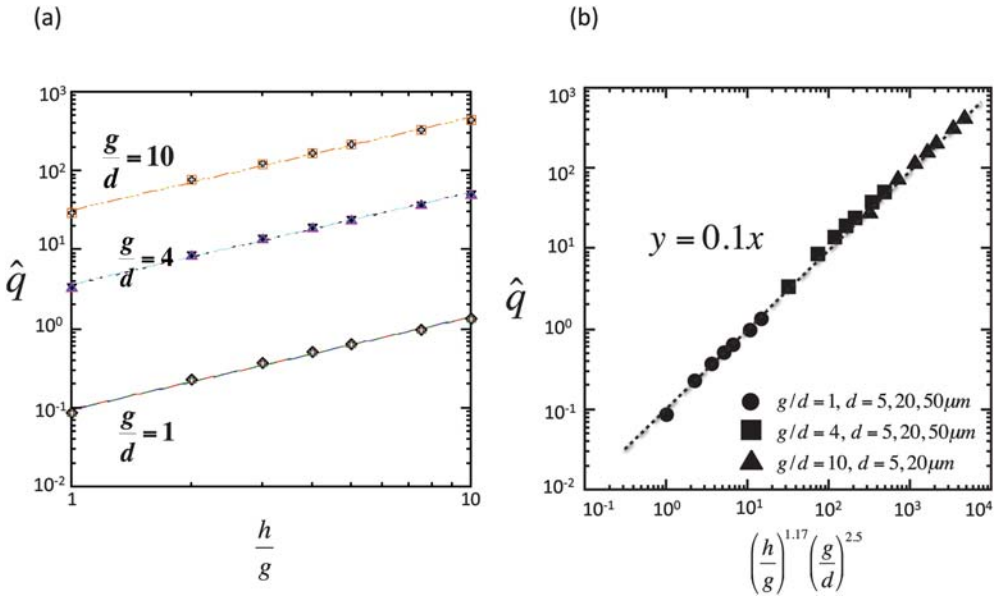

Fig. 3 Dimensional analysis for viscous, low Reynolds number flow around a post. (a) The dimensionless flow rate per unit width, $\hat{q}$, is plotted as a function of the dimensionless parameter h/g for different ratios of g/d. Flow rate computed from the COMSOL numerical model is used to calculate $\hat{q}$. For each g/d, three diameters (5, 20 and 50 μm) were simulated. Although three separate curves are obtained, each of the curves has the same slope. **(b)** $\hat{q}$ is plotted as function of a dimensionless parameter, such that all the simulated data from Fig. 3**a** collapses to a master curve. 3 different diameters were simulated for $g/d = 1$ and 4 and two diameters for $g/d = 10$.

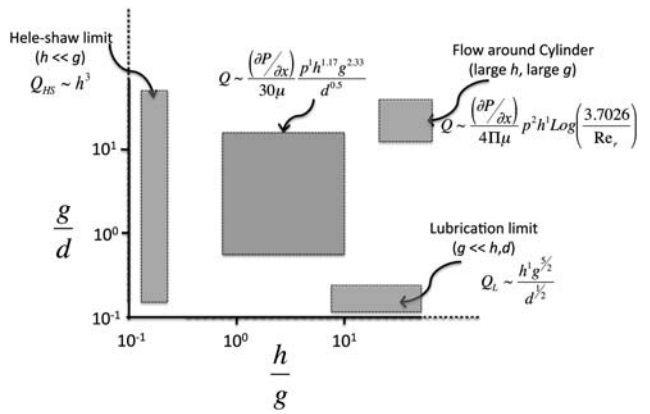

Fig. 4 Comparison of the viscous scaling for flow through a lattice of posts with limiting regimes. The solid square in the middle shows the design space for our experiments and numerical simulations. The surrounding, smaller boxes show the limiting scenarios.

$$Q_L \sim \frac{h^1 g^{5/2}}{d^{1/2}} \tag{4}$$

Comparing eqn (3) and (4), notice the same inverse square root dependence on the pillar diameter and the nearly similar dependencies on pillar height and diameter. Undoubtedly, the physics of the flow in the parameter range that has been investigated is qualitatively similar to lubrication flow; most of the pressure drop occurs as the liquid gets squeezed between the posts. Eqn (4) is not accurate for $h/g \sim 10$, where the lubrication approximation breaks down and the error can be as much as 50%.

Eqn (3) also shows some similarity to the pressure-driven flow around an isolated infinite pillar. In this case, the pillar is infinite and therefore the viscous drag arises entirely from the surface of the pillar given by the drag coefficient,[4] $C_D \sim \log\left(\frac{3.7026}{\mathrm{Re}_r}\right)$. The flow extends infinitely in all three directions, but to compare with our scaling model we calculate the flow through a cross-sectional area p^*h around the post which is found to be $Q \sim \frac{\left(\partial P/\partial x\right)}{4\Pi\mu}p^2h^1Log\left(\frac{3.7026}{\mathrm{Re}_r}\right)$. Upon comparing to eqn (3), a similar dependence on the height is noticed. Fig. 4 summarizes the comparison of our scaling with these limiting regimes.

To understand the wetting behavior of the post structure, the scaling for viscous flow in eqn (3) is combined with capillary pressure in eqn (1). The pressure gradient $\partial P/\partial x$ is taken as $\Delta P_{\mathrm{cap}}/l$ and experimentally measured velocity as $\frac{dl}{dt} = \frac{q}{h} \cdot \frac{p}{p_{eff}}$, where $p_{eff} = p - \frac{\pi d^2}{4p}$ is the effective spacing between the posts that the flow experiences (see Supplemental **B** for details†). We thus obtain the following.

$$\frac{dL}{dt} = \frac{1}{30l} \cdot \frac{\gamma}{\mu} \cdot \frac{g^{1.33}}{p_{eff}\, h^{0.83} d^{0.5}}\left[\cos\theta\left(\pi\, d\, h + p^2 - \frac{\pi d^2}{4}\right) - \left(p^2 - \frac{\pi d^2}{4}\right)\right] \tag{5}$$

For complete wetting ($\cos\theta = 1$), eqn (5) is integrated to obtain the total length of the liquid front as a function of time and shown to follow Washburn dynamics.

$$L = \sqrt{\frac{\pi\,\gamma}{15\mu} \cdot \frac{g^{1.33} h^{0.17} d^{0.5}}{p_{eff}}\, t} \tag{6}$$

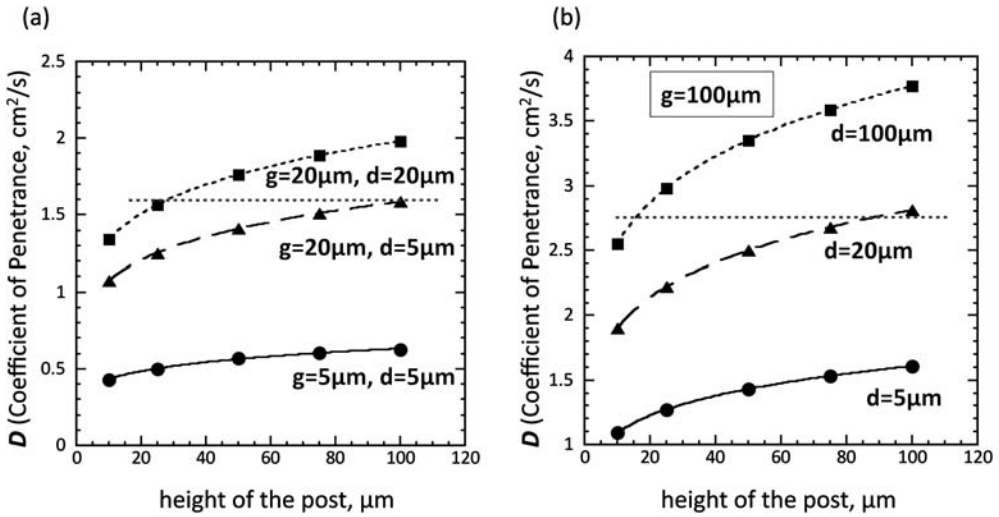

Fig. 5 Simulation results from the unified scaling model. The numerical model predicts the coefficient of penetrance, D, for different configurations of pillar arrays. **(a)** D as a function of height for various combinations of gap and diameter. **(b)** D as a function of height for constant gap, but varying diameter of the posts. The dotted line in the plot emphasizes how different combinations of (h, d, g) can end up giving the same D—this would have interesting implications for fabrication.

Fig. 5 summarizes a few design predictions using the unified scaling model (eqn (5)). The coefficient of penetrance, D is plotted as a function of post height, h. It is evident that D, and therefore the rate of spreading, increases with increasing h. However, this effect is more prominent at smaller h while for taller posts, the coefficient D tends to plateau. These findings are in agreement with previous experimental findings[6] and consistent with the hypothesis that for taller posts the gain in capillary pressure is counter-balanced by the increase in viscous drag due to increased surface area. Fig. 5a shows the coefficient, D for different combinations of g and d as we increase h. Fig. 5b shows the coefficient D for same gap g but different diameter, d. The plots give interesting insights for optimizing D. For example, consider two cases both with a gap $g = 20$ μm. The same value of D is obtained for $h = 100$ μm & $d = 5$ μm and for $h = 20$ μm & $d =$ 20 μm (shown by a dotted horizontal line in Fig. 5a).

Experiments

Wetting experiments were conducted on a 3 cm × 3 cm lattice of posts etched in silicon using the Bosch deep reactive ion etching process (Fig. 1). Devices with three different posts heights were fabricated (20, 40 and 60 μm). Prior to wetting, silicon devices were gently cleaned with acetone, isopropyl alcohol, and deionized water and treated with UV radiation for one minute (UVO Cleaner, Jelight Company Inc., Irvine CA). Experiments were performed on a Nikon zoom microscope (AZ100) and recorded with a digital camera (Nikon Digital Sight). Movies of experiments were analyzed using an image analysis macro in *ImageJ* (available from NIH, http://rsbweb.nih.gov/ij/).

A 40μL drop of deionized water is placed at the edge of the silicon device (Fig. 6a). Capillary pressure spontaneously draws the liquid into the posts and the length of the maximum liquid front, L is monitored with time, t (Fig. 6b) for varying height, h. We fit the data of length L with $t^{1/2}$ and obtained a regression coefficient R^2 greater than 0.996—thus validating that the

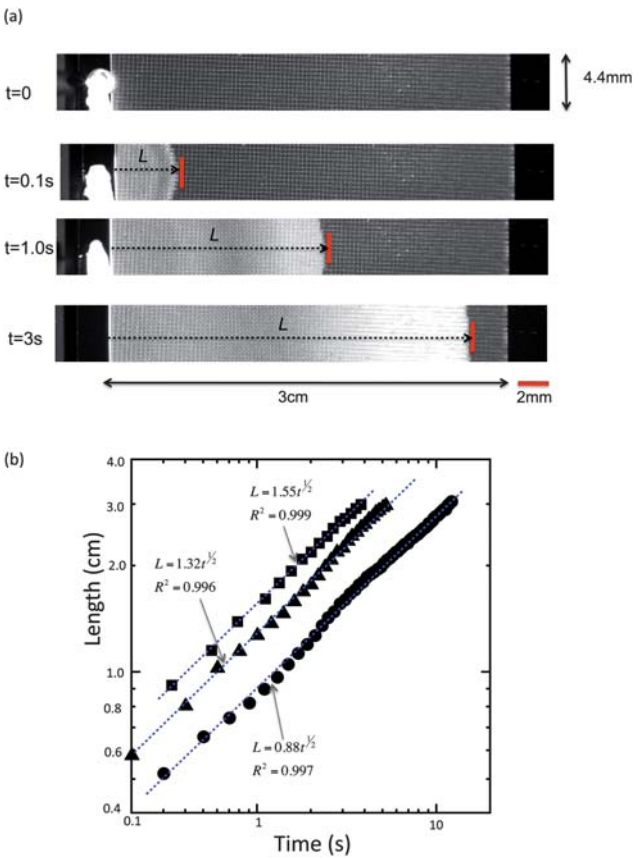

Fig. 6 Wetting experiments in microfabricated silicon posts follow Washburn dynamics. (a) The silicon device is 3 cm wide and contains a square lattice of posts ($g = 50$ μm, $d = 100$ μm). A 40 μL drop of water is added to the left edge of the device. The sequence of images shows the progression of wetting and the increasing length, L, of the moving liquid front. **(b)** Plot of L *vs.* time, t. We were able to fit the data to a power law function with an exponent of ½ with a regression coefficient greater than 0.996. The dotted line is the power law fit and confirms Washburn dynamics.

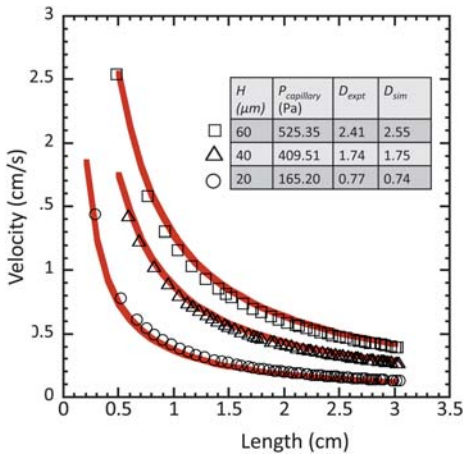

Fig. 7 Wetting on silicon pillars validate unified scaling model. The result from the unified numerical model is plotted (solid lines) along with the experimental data for three different heights of the posts (short, medium and tall). A contact angle of 43° was used for all three devices. The coefficient of penetrance, D, was predicted within 8% for each of the three devices. It may be noted that 43° was used arbitrarily and the error is substantially reduced to within 1% if we change the contact angle in each device individually by ±2°. Here $d = 100$ μm and $g = 50$ μm.

imbibing liquid front indeed follows a planar front and agrees with Washburn dynamics. Using the fitted curve, the coefficient of penetrance, D, is measured to be 2.41 cm^2 s^{-1} for $d = 100$ μm, $g = 50$ μm and $h = 60$ μm. Furthermore, the edge velocity of the liquid front is calculated as $v = \frac{dL}{dt} = \frac{D}{2}\frac{1}{L}$ and is shown in Fig. 7. The edge velocity at 3 cm is found to be 5 mm s^{-1}. As the length of the penetrated liquid grows, the pressure gradient driving the flow decreases and so the edge velocity also drops.

Fig. 7 shows the validation of the unified scaling model (eqn (5)) with wetting experiments using water on silicon microposts. The experimentally measured L *vs.* t from three different sets of devices is compared to the predictions from eqn (5). A contact angle of 43° was estimated for all devices. The use of this contact angle is consistent with others in the field and specifically with the contact angle resulting from the Bosch process of etching silicon.[9–11] The contact angle on etched silicon has been reported in the literature to be between 35 and 43°. Using a contact angle of 43°, the experimentally obtained L *vs.* t shows excellent agreement with numerical predictions. The table in Fig. 7 lists the values of the coefficient of penetrance, D, obtained from experiments and numerical simulations. These data agree to within 8%. Since the contact angle will vary slightly from device to device, a part of this error can be attributed to the variation in contact angle. The error in D is less than 1% when the contact angle is allowed to vary by ±2° between devices.

Conclusions

A combination of numerical simulations and dimensional analysis was used to derive a scaling model for predicting flow through an array of microposts. It was found that the flow rate per unit gap between two adjacent pillars in an array scales as $h^{1.17}$, $d^{-0.5}$ and $g^{1.33}$. This universal scaling was accurate to within ~8% over a wide parameter space that spanned $5 < d < 50$ μm, $1 < g/d < 10$, and $1 < h/g < 10$. This parameter space is wide enough to encompass geometries that are most commonly used in lab-on-a-chip applications.

In addition, the scaling model was extended to wetting by incorporating the expression for the capillary pressure through an array of posts. The resulting unified model, which combines viscous drag and capillary pressure, can thus be used in the design of posts with the appropriate combination of h, d and g to obtain the desired rate of wetting. It was found that the same rate of penetrance may be obtained using different combinations of h, d and g as shown with dotted horizontal lines in Fig. 5a and b. For instance, the same coefficient of penetrance may be obtained with much shorter pillars by choosing the appropriate diameter and spacing. Such predictions are critical from a microfabrication standpoint, particularly because fabricating deeper (taller) posts is usually harder than making wider posts.

Wetting experiments using microfabricated posts in silicon were performed to validate the unified scaling model. Our scaling model predicts the coefficient of penetrance, D, to within 8% of the experimental values. This 8% disagreement may be attributed partially to variation in contact angle. If the contact angle is allowed to vary by ±2° between devices, the penetrance D agrees with experiments to within 1%. The numerical model is now being extended to include other arrangements of posts (triangular array, staggered *etc.*), non-uniform variation in gap and diameter. Such predictions will not only be a useful tool for designing lab-on-a-chip devices but will also advance our understanding of the physics of flow around a post.

Acknowledgements

We would like to acknowledge funding support from DARPA TGP program (grant N66001-08-1-2035) for this work.

References

1 H. H. Cui and K. M. Lim, *Langmuir*, 2009, **25**, 3336–3339.
2 S. Nagrath, L. V. Sequist, S. Maheswaran, D. W. Bell, D. Irimia, L. Ulkus, M. R. Smith, E. L. Kwak, S. Digumarthy, A. Muzikansky, P. Ryan, U. J. Balis, R. G. Tompkins, D. A. Haber and M. Toner, *Nature*, 2007, **450**, 1235–1239.
3 B. He, N. Tait and F. Regnier, *Anal. Chem.*, 1998, **70**, 3790–3797.
4 H. Lamb, *Hydrodynamics*, New York Dover Publications, 1945.
5 H. Hasimoto, *J. Fluid Mech.*, 1959, **5**, 317–328.
6 C. Ishino, M. Reyssat, E. Reyssat, K. Okumura and D. Quere, *Europhys. Lett.*, 2007, **79**, 56005.
7 E. W. Washburn, *Phys. Rev.*, 1921, **17**, 273–283.
8 L. Leal, *Advanced Transport Phenomena: Fluid Mechanics and Convective Transport Processes*, Cambridge University Press, Cambridge, 2007.
9 M. C. Gomes, A. C. Fernandes, B. S. Almeida and R. M. Almeida, *J. Mater. Sci.*, 1995, **30**, 3893–3896.
10 S. B. Jo, M. W. Lee, S. G. Lee, E. H. Lee, S. G. Park and B.-H. O, *J. Vac. Sci. Technol., A*, 2005, **23**, 905–910.
11 S. B. Jo, M. W. Lee, S. G. Park, J. K. Suh and O. Beom-Hoan, *Surf. Coat. Technol.*, 2004, **188–189**, 452–458.

